Magnetism of amorphous iron: From ferromagnetism to antiferromagnetism and spin-glass behavior

I. Turek* and J. Hafner
Institut für Theoretische Physik, TU Wien, Wiedner Hauptstrasse 8-10, A-1040 Wien, Austria
(Received 15 January 1992)

The magnetization of realistic structural models of amorphous iron is calculated self-consistently within the framework of local-spin-density theory. We show that the distribution of the magnetic moments is strongly coupled to fluctuations in the local self-consistent potential. At a density slightly lower than bcc Fe, amorphous iron is predicted to be a strong inhomogeneous ferromagnet. An increase in density leads to a broadening of the bands and a transition to weak magnetism. The transition from strong to weak magnetism is coupled with the appearance of a few negative moments. Further compression induces more spin flips, leading to a substantial antiferromagnetic component in the magnetic polarization. At large compressions, the global magnetovolume effect leads to a reduction of all magnetic moments. The distribution of positive and negative moments overlaps, resulting in a transition to a spin-glass state. Our calculations demonstrate a universal proportionality of the local magnetic moment and the local exchange splitting.

I. INTRODUCTION

Recently, there has been considerable interest in the investigation of the magnetic properties of the metastable (amorphous, face-centered-cubic, hexagonal-close-packed) phases of iron. This interest would be rather academic, were it not for advances in the experimental techniques for growing thin films and to control interfaces at an atomic scale, which has opened possibilities to synthesize metastable metallic structures.[1-5] The magnetic ground state of the crystalline phases has been studied repeatedly using electronic-structure calculations based on local-spin-density (LSD) functional theory.[6,7] For the stable body-centered-cubic (bcc) form the ferromagnetic state was found to have the lowest energy at all densities.[8,9] For the metastable face-centered-cubic (fcc) and hexagonal-close-packed (hcp) phases the LSD calculations yield a nonmagnetic zero-pressure state, but a transition to an antiferromagnetic state in an expanded lattice, followed by a high-spin ferromagnetic state at even lower densities.[9-12] Most recent results suggest that the transition from the antiferromagnetic to the ferromagnetic state might occur via a noncollinear spin structure, possibly a spiral spin state.[13]

On the other hand, the magnetic properties of amorphous iron remain controversial. Early investigations suggested a uniform reduction of ferromagnetism as a consequence of structural disorder,[14] recent results on dilute Fe_xM_{1-x} (M =Zr,Y,La,Ce,Lu,...) alloys have been interpreted in terms of a transition to a spin-glass state after the disappearance of ferromagnetism with increasing Fe content.[15-17] However, this view has not gone unchallenged: alternatively, amorphous Fe has been described as asperomagnetic (i.e., as a random noncollinear spin structure with a nonzero net moment)[18] or mictomagnetic (i.e., forming magnetic clusters).[19] The first step in understanding the magnetism in amorphous metals consists in the investigation of the electronic structure. There have been a number of spin-polarized calculations of the electronic density of states (DOS) for amorphous iron, based on more or less realistic structural models.[20-23] However, these calculations are of different quality than the self-consistent LSD calculations for the crystalline phases: all are based on parametrized tight-binding (TB) Hamiltonians and are either non-self-consistent or achieve self-consistency only within the restricted framework of a TB theory for a Hubbard Hamiltonian with a site-independent U. The various TB calculations agree in predicting an inhomogeneous ferromagnetic state for amorphous iron, with an average moment that is nearly as high as in bcc iron. Krauss and Krey[22] discussed global and local magnetovolume effects and predicted a global volume dependence of the average ferromagnetic moment that agrees with the volume dependence of the antiferromagnetic moment predicted for the fcc phase.[10] To our knowledge, no spin-polarized electronic structure calculation has succeeded in generating the true spin-glass state of amorphous iron expected from the extrapolation of the magnetic properties of dilute magnetic alloys and predicted by Kakehashi's theory of the local-environment effect.[17]

In this paper we present a locally self-consistent calculation of the spin-polarized electronic structure of amorphous Fe. A structural model for amorphous iron is generated by a simulated molecular-dynamics (MD) quench based on interatomic forces calculated within a hybridized nearly-free-electron tight-binding-bond approach (NFE-TBB).[24,25] Models with more than 1000 atoms per cell are generated for the analysis of the diffraction data; models with 64 atoms per cell serve as the basis for the self-consistent electronic-structure calculations using a linear-muffin-tin-orbital[26-29] (LMTO) supercell technique. The self-consistent solution takes full account of the local fluctuations in the spin density and in the effective one-electron potentials. The importance of these local fluctuations appears very clearly in the distribution

of the local moments: although the average magnetic moment is predicted to decrease under compression, as has also been found in previous TB calculations, we find a pronounced change of the local-moment distribution, which has not been predicted before. With increasing compression, amorphous iron shows a transition from an inhomogeneous ferromagnetic state over an antiferromagnetic to a spin-glass state.

The investigation of the local fluctuations in the electronic DOS and in the self-consistent atomic potentials is very elucidating. We find that in the ferromagnetic regime the small band width leads to strong magnetism; the gradual transition to antiferromagnetic behavior is correlated with the broadening of the bands and a transition to weak magnetism.

This interpretation is supported by a series of self-consistent spin-polarized electronic-structure calculations for models of amorphous Co. We find that over a wide range of densities amorphous Co is a strong, slightly inhomogeneous ferromagnet. Only at rather high compression, when the band width is so large that the Stoner criterion can no longer be satisfied, does a transition to a nonmagnetic state occur.

Our paper is arranged as follows. In Sec. II we review very briefly the construction of the structural model for amorphous iron and cobalt. Details of the LSD calculation are given in Sec. III. The distributions of the local magnetic moments are described in Sec. IV. Local and global magnetovolume effects are discussed in Sec. V. Correlations between the local magnetic moment and the local density of states are investigated in Sec. VI, and the magnetic exchange splitting is investigated in Sec. VII. Our conclusions are presented in Sec. VIII.

II. STRUCTURAL MODELING

Structural models for amorphous iron and cobalt have been prepared by a simulated molecular-dynamics quench. Interatomic forces have been calculated using a hybridized nearly-free-electron tight-binding-bond approach.[24,25] The basic assumption is that the total energy may be divided into contributions from s and d electrons. Pseudopotential theory is used to express the s-electron contribution in terms of volume and pair forces. The d-electron contribution to the interatomic forces is described in terms of a tight-binding model. The attractive forces resulting from the strong covalent d-d interactions are expressed in terms of the d-d transfer integrals, and the bond order, which is defined as the difference in the number of electrons in bonding and antibonding d states. The d-d interactions depend on the atomic environment via the bond order. If the bond order is calculated in a Bethe-lattice approximation, the interatomic potential reduces to a weakly coordination-number-dependent pair potential. This pair interaction is strongest for a half-filled d band. Details of the theory are given in Ref. 25; applications to the molecular-dynamics simulation of liquid transition metals (including iron and cobalt) are described in Ref. 30.

The molecular dynamics simulations are performed in the microcanonical ensemble. The simulation is started in the liquid phase (where the calculated pair-correlation function agrees well with the diffraction data), the system is quenched at a rate of approximately 10^{15} K/s to $T = 50$ K, followed by a slower quench to $T = 4$ K, at a density that is slightly lower than that of natural bcc Fe. This initial configuration is homogeneously compressed in several steps and reequilibrated after each compression. Note that the quench has to be made to this very low temperature and at a high quench rate. A somewhat slower (10^{12} K/s) quench results in a distorted crystalline (fcc) configuration, as expected for the ground state of nonmagnetic iron. However, a perfect fcc crystal is formed only if the periodic boundary conditions are compatible with the crystalline lattice.

We perform two independent MD runs: one for a large ensemble with $N = 1458$ particles and one for a small ensemble for $N = 64$ particles. The large ensemble is used to produce a pair-correlation function for comparison with the available experimental data.[31] It also allows us to verify that the simulations for the small ensemble

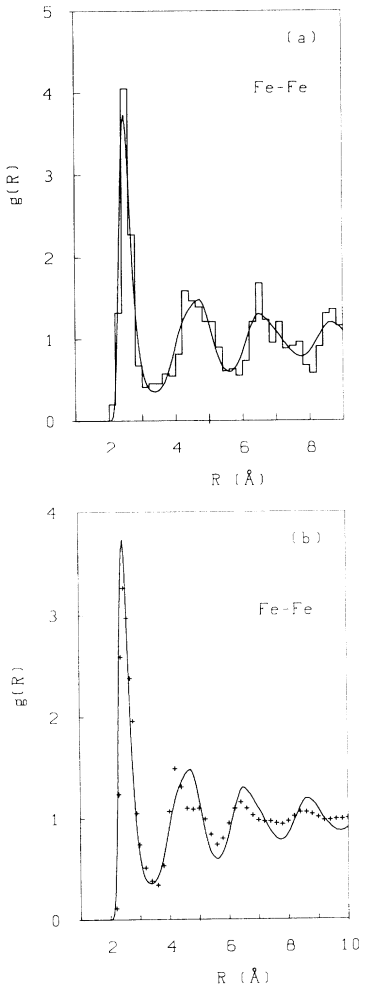

FIG. 1. Pair-correlation function $g(r)$ for amorphous iron, as calculated from an ensemble average over a 1458-atom model (solid line) and for a single 64-atom configuration (histogram) (a), compared with the experimental data (b) (after Ref. 31).

are not seriously affected by the periodic boundary conditions. Figure 1 compares the ensemble-averaged pair-correlation function for the large ensemble with that calculated for a single 64-atom configuration and with the experimental data.

III. SPIN-POLARIZED ELECTRONIC-STRUCTURE CALCULATIONS

Once a periodic model has been constructed, the calculation of the spin-polarized electronic structure proceeds in the same way as for a very complex crystal with a simple-cubic structure.[28,29] However, even today self-consistent band-structure calculations for systems with 64 atoms in the periodically repeated cell are nontrivial and require a very efficient computational technique. We adopted the scalar relativistic linear-muffin-tin-orbital method in the atomic-sphere approximation (LMTO-ASA).[26,27] Exchange and correlation are described in the local-spin-density approximation.[6,7] The LMTO-ASA is ideally suited for amorphous transition metals because of their rather high packing density.

In the LMTO, the Schrödinger equation for an electron wave function u_{RL} within the atomic sphere centred at the site R may be formulated as[32]

$$\sum_{R',L'} [P_{RL}(E)\delta_{RL,R'L'} - S_{RL,R'L'}] N^{-1}_{R'L'}(E) u_{R'L'} = 0, \tag{1}$$

where S is a structure constant matrix and P a diagonal potential function matrix (N is a normalization function, L stands for the set of angular momentum l, magnetic m, and spin σ, quantum numbers). A conventional parametrization of the potential function is

$$P_{RL}(E) = \left[\frac{\Delta_{RL}}{E - C_{RL}} + \gamma_{RL}\right]^{-1}, \tag{2}$$

with the potential parameters describing the center, $C_{Rl\sigma}$, the width, $\Delta_{Rl\sigma}$, and the distortion, $\gamma_{Rl\sigma}$, of the "pure" $Rl\sigma$ band.

In the supercell approach the local potential parameters are determined self-consistently. This is very important as we shall show that there is a unique correlation between the local potential and the local moment. This correlation is necessarily obscured in calculations treating self-consistency in an approximate way.

The most serious limitation of the supercell approach is the relatively small number of particles in the cell. For simple-metal glasses we have demonstrated,[33] via a comparison of the **k**-space LMTO calculations for a 64-atom model with the **r**-space tight-binding LMTO recursion calculation for an 800-atom model (both calculations use the same one-electron potential) that the supercell calculation is not seriously limited by the boundary conditions. As in the **r**-space recursion calculations, self-consistency can be easily achieved only for an average atom; we prefer the **k**-space calculation that allows us to achieve local selfconsistency on each atomic site.

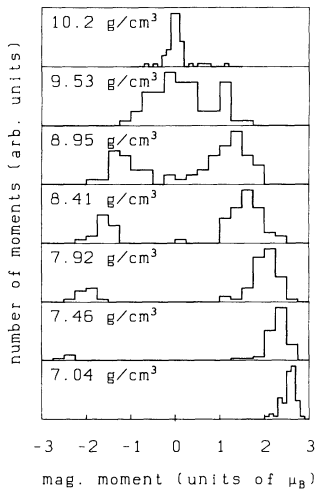

FIG. 2. Distribution of the local magnetic moments in amorphous iron at densities varying between $\rho = 7.04$ g/cm^3 and $\rho = 10.2$ g/cm^3; see text.

IV. DISTRIBUTION OF MAGNETIC MOMENTS

The calculated distributions of the magnetic moments in amorphous iron at different densities, and the variation of the average magnetic moment with density are shown in Figs. 2 and 3. The predicted variation of the average magnetic moment $\bar{\mu}$ with the atomic volume V is rather similar to the μ-V relation calculated for the antiferromagnetic phase of fcc iron. Differences appear only at the lowest density, where the average moment for amorphous iron lies between the moments predicted for the antiferromagnetic and the high-spin ferromagnetic state of fcc Fe, and at the highest density, where fcc Fe is nonmagnetic, whereas the amorphous phase still has a

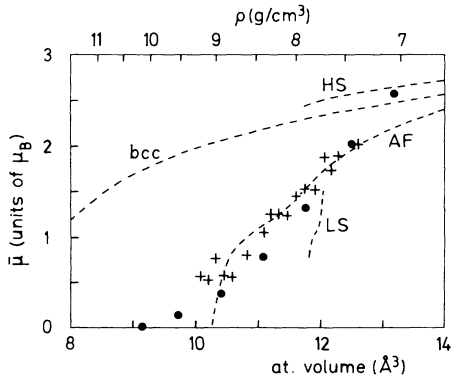

FIG. 3. Variation of the average magnetic moment $\bar{\mu}$ of amorphous iron with density: full dots—present results, and crosses—tight-binding calculations of Krauss and Krey (Ref. 22). For comparison we show the density dependence of the magnetic moment in ferromagnetic bcc iron and in ferromagnetic and antiferromagnetic fcc iron as calculated by Moruzzi, Marcus, and Kübler (Ref. 10, the labels HS and LS refer to the high-spin and low-spin solutions for ferromagnetic fcc Fe).

small net moment. On the other hand, there is no similarity with the ferromagnetic state of bcc Fe. This is not unexpected, since the local arrangement in a-Fe is close packed.

Our results for the $\bar{\mu}$-V relation for amorphous iron agree rather well with those obtained by Krauss and Krey[22] on the basis of a parametrized TB Hubbard Hamiltonian. However, if the average moments agree, there are substantial differences in their distributions. At low densities, Krauss and Krey calculate a broad distribution with a standard deviation of about $0.5\mu_B$, centered at $\bar{\mu} \sim 2.0\mu_B$. Upon compression, $\bar{\mu}$ is shifted to lower moments, and there is slight increase in the standard deviation. At the highest density ($\rho \sim 9$ g/cm^3) they find a broad unimodular distribution centered at $\bar{\mu} \sim 0.6\mu_B$ and overlapping into the region of negative local moments. Thus at all densities, the magnetic state of amorphous iron is described as that of an inhomogeneous ferromagnet.

Our calculations lead to an entirely different picture: at the lowest density, we find an inhomogeneous ferromagnetic state with a rather narrow distribution around a large average moment close to the magnetic moment in bcc iron, $\bar{\mu} \sim 2.3\mu_B$. At a density of $\rho \sim 7.5$ g/cm^3 (corresponding roughly to the density of sputter-deposited amorphous iron), some sites acquire a large negative moment. Upon further compression, more sites switch the magnetic moment, the centers of gravity of the two distributions shifting to slightly smaller absolute values. Only at a density of $\rho \sim 8.4$ g/cm^3 do a small number of low-moment states appear. At still higher densities, the distributions of the negative and positive moments begin to overlap, and at a density of $\rho \sim 9.5$ g/cm^3 we find a broad distribution of magnetic moments with nearly zero net magnetization. Upon further compression, this distribution narrows, indicating that ultimately a transition to a nonmagnetic state will occur. Thus we find a transition from an inhomogeneous ferromagnetic state via an incompletely antiferromagnetic to a spin-glass state.

On the other hand, amorphous cobalt (Fig. 4) is predicted to be ferromagnetic over a wide range of densities, with a narrow distribution of the magnetic moments around a mean value that is only slightly lower than predicted for hcp Co [$\bar{\mu} = 1.55\mu_B$ (Ref. 34) and $\bar{\mu} = 1.60\mu_B$ (Ref. 35)] and for fcc Co [$\bar{\mu} = 1.58\mu_B$ (Ref. 34), $\bar{\mu} = 1.56\mu_B$ (Ref. 36), and $\bar{\mu} = 1.56\mu_B$ (Ref. 37)]. Under compression, the magnetovolume effect leads to a slow reduction of the average magnetic moment, and at a compression of 30% (compared to hcp Co at equilibrium), a transition to a nonmagnetic state is predicted (Fig. 5).

The detailed magnetic structure of a-Fe is illustrated in Fig. 6 in the form of a projection of the model structure on the (x, z) plane, the size and direction of the magnetic moment being indicated by arrows. The atomic structure is changed only very slightly upon compression—this allows us to follow the variation of individual moments with density. We see immediately that the change from positive to negative moment at a given site is not a gradual one; rather a large moment flips from up to down with only small changes in the moments of the surrounding sites. We also note that the first negative moments appear at large distances from each other. Only at a concentration of nearly 30% negative moments, do negative moments at nearest-neighbor sites appear.

It is interesting to have a brief look at the distribution of the magnetic moments in quench-condensed crystalline Fe. As mentioned above, a "slow" quench produces a close-packed crystalline structure. However, a cubic MD cell with 64 atoms is not compatible with a perfect fcc lattice. Therefore, the quench results in a distorted close-packed structure. Each atom has twelve nearest neighbors (four at 2.46 Å, two at 2.55 Å, four at 2.60 Å, and two at 2.70 Å, compared to the ideal close-packing distance of 2.548 Å). A spin-polarized supercell calculation yields an antiferromagnetically polarized structure, with magnetic moments of $\pm 1.73\mu_B$. Out of the twelve nearest neighbors of a given spin, four spins are oriented parallel and eight antiparallel to the spin of the central atom. Both the magnitude of the spins and the nearest-neighbor correlation correspond closely to that predicted for fcc Fe with a AuCu-I-type antiferromagnetic structure.[10] The point is that in conventional

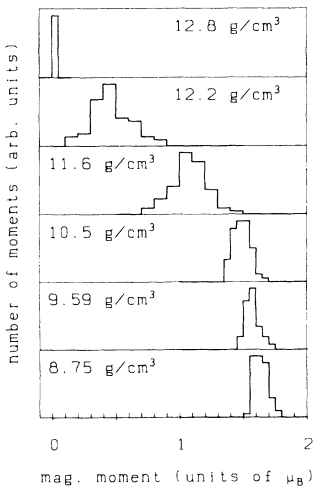

FIG. 4. Distribution of the local magnetic moments in amorphous cobalt at densities varying between $\rho = 8.75$ g/cm^3 and $\rho = 12.8$ g/cm^3.

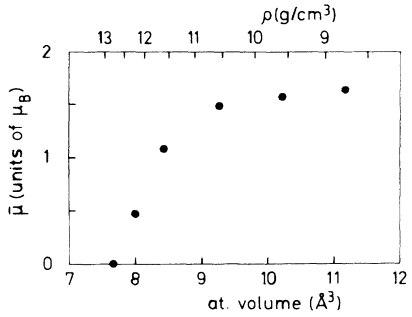

FIG. 5. Variation of the average magnetic moment in amorphous Co with density.

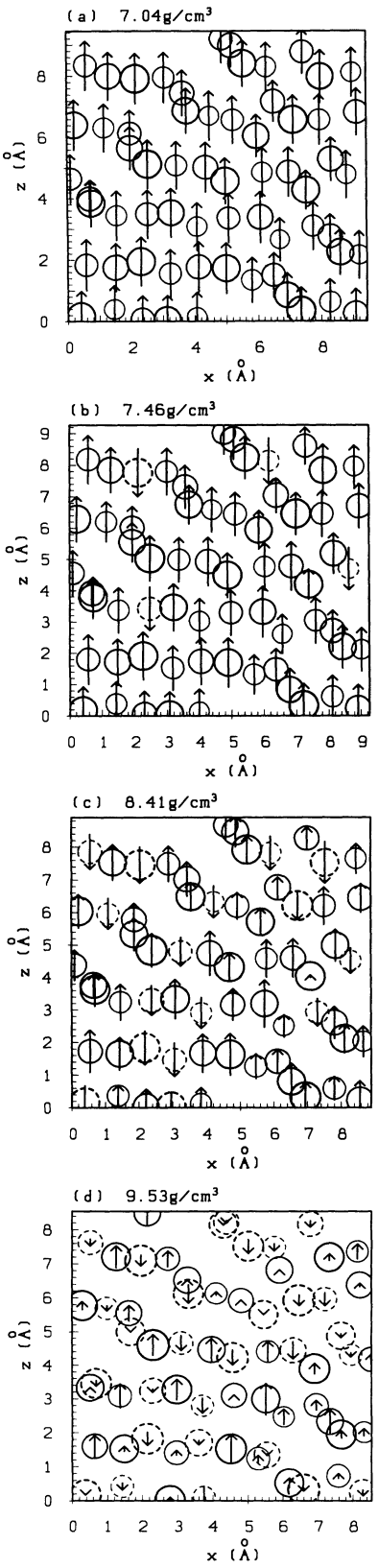

FIG. 6. (a)–(d) Projections of the 64-atom models for amorphous iron into the (x, z) plane. The size of the circles representing the atoms is scaled with the y coordinate, the arrows indicate the magnitude and direction of the local magnetic moment.

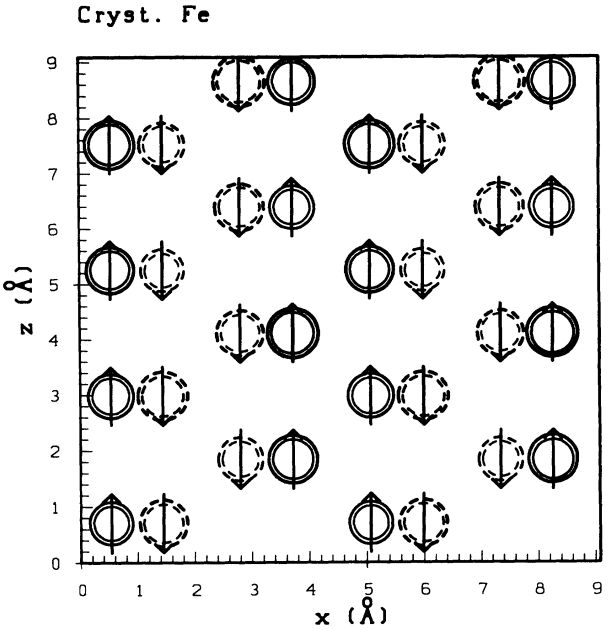

FIG. 7. Projection of the spin configuration calculated for a crystalline structure produced by a slow molecular-dynamics quench (see text).

spin-polarized electronic-structure calculations the type of antiferromagnetic symmetry breaking has to be assumed *a priori*. No such restrictions apply to our supercell calculations. The possibility to investigate complex spin structures in crystalline lattices deserves further investigation (possible supercells for a fcc lattice contain 32 or 108 atoms). A projection of the magnetic structure produced by slow quenching is shown in Fig. 7.

V. LOCAL MAGNETOVOLUME CORRELATIONS

It has been suggested that the local fluctuations of the magnetic moments are closely related to fluctuations in the local density. The local density of an amorphous network may be characterized either in a purely geometric way, by the volume of the Voronoi polyhedron constructed around each site,[38,39] or in a more physical way in terms of the atomic level pressures.[40,41] The correlation between the local magnetic moment and the volume of the Voronoi polyhedron is shown in Fig. 8 for three different densities. At not too high densities, there is indeed a correlation between the magnetic moment and the local volume: a large volume corresponds to a large magnetic moment and a small volume to a small magnetic moment. However, this correlation applies equally to sites with positive and negative moments, so that the magnetovolume correlation alone is not sufficient to explain the appearance of antiferromagnetic exchange interactions under compression. Moreover, at higher densities the correlation between volume and moment becomes rather diffuse.

A similar conclusion arises from the investigation of the correlation between magnetic moment and the atomic level pressure. In a system of interacting atoms, the application of a small uniform strain $\epsilon^{\mu\nu}$ will result in a change in energy. The change in energy associated with the lth atom is given to first order by[40–42]

$$\Delta E_l = \Omega_l \sum_{\mu,\nu} \sigma_l^{\mu\nu} \epsilon^{\mu\nu}, \tag{3}$$

where the $\sigma_l^{\mu\nu}$ are the components of the atomic level stress tensor. The individual components depend on the choice of a coordinate system, so one has to consider the invariants of the stress tensor, i.e., the local hydrostatic pressure defined in terms of the trace of $\sigma_l^{\mu\nu}$,

$$p_l = \frac{1}{3} \sum_{\nu} \sigma_l^{\nu\nu}, \tag{4}$$

and the von Mises shear stress. For explicit expressions for $\sigma_l^{\mu\nu}$ in terms of the interatomic interactions, see Refs. 40–42.

The correlation between the atomic level pressure and the local magnetic moment is shown in Fig. 9. The conclusion to be drawn is again very similar: at lower densities there is a clear correlation between a high atomic level pressure and a small absolute value of the magnetic moment, but no evident distinction between spin-up and spin-down sites. There is also no correlation between the magnetic moment and the coordination number or the

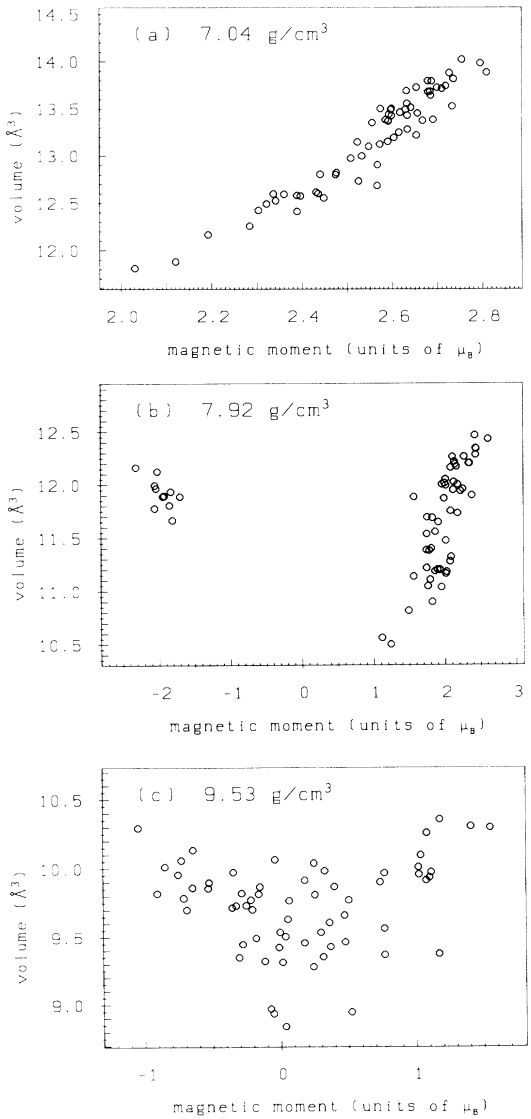

FIG. 8. Plot of the local magnetic moment μ_l against the local volume (the volume of the Voronoi polyhedron at the site l) in amorphous iron for three different densities: $\rho = 7.04$ g/cm^3 (a), $\rho = 7.92$ g/cm^3 (b), and $\rho = 9.53$ g/cm^3 (c). Note the change of scale for the magnetic moments.

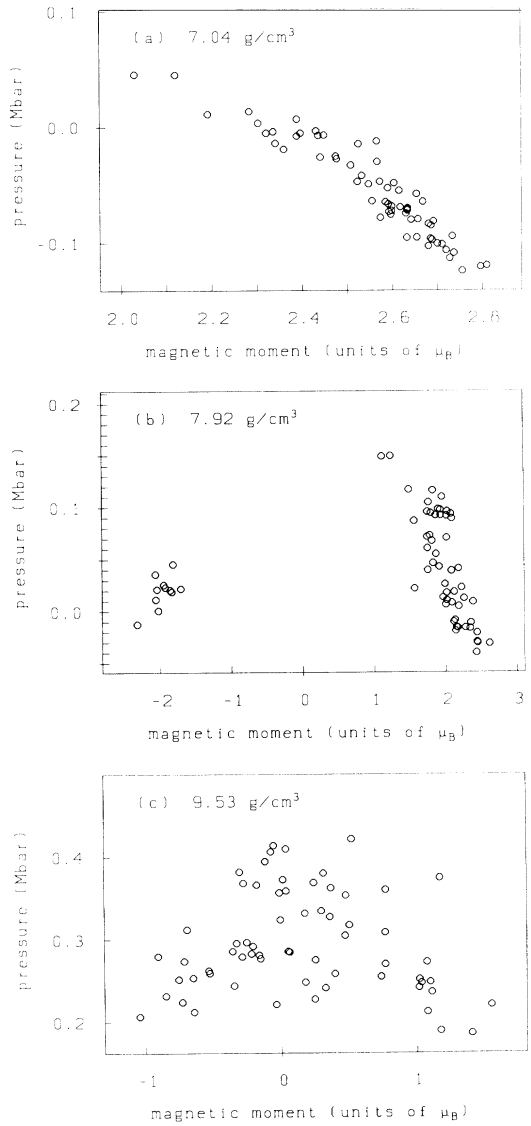

FIG. 9. Plot of the local magnetic moment μ_l against the atomic level pressure p_l in amorphous iron for three different densities (cf. Fig. 8).

distribution of the bond angles.

The conclusion is that to find an explanation for the appearance of antiferromagnetic couplings we have to look more closely into the local fluctuations in the electronic states and potentials.

VI. LOCAL ELECTRONIC DENSITIES OF STATES

Figure 10 shows the spin-polarized local densities of states, averaged over sites with positive and negative mo-

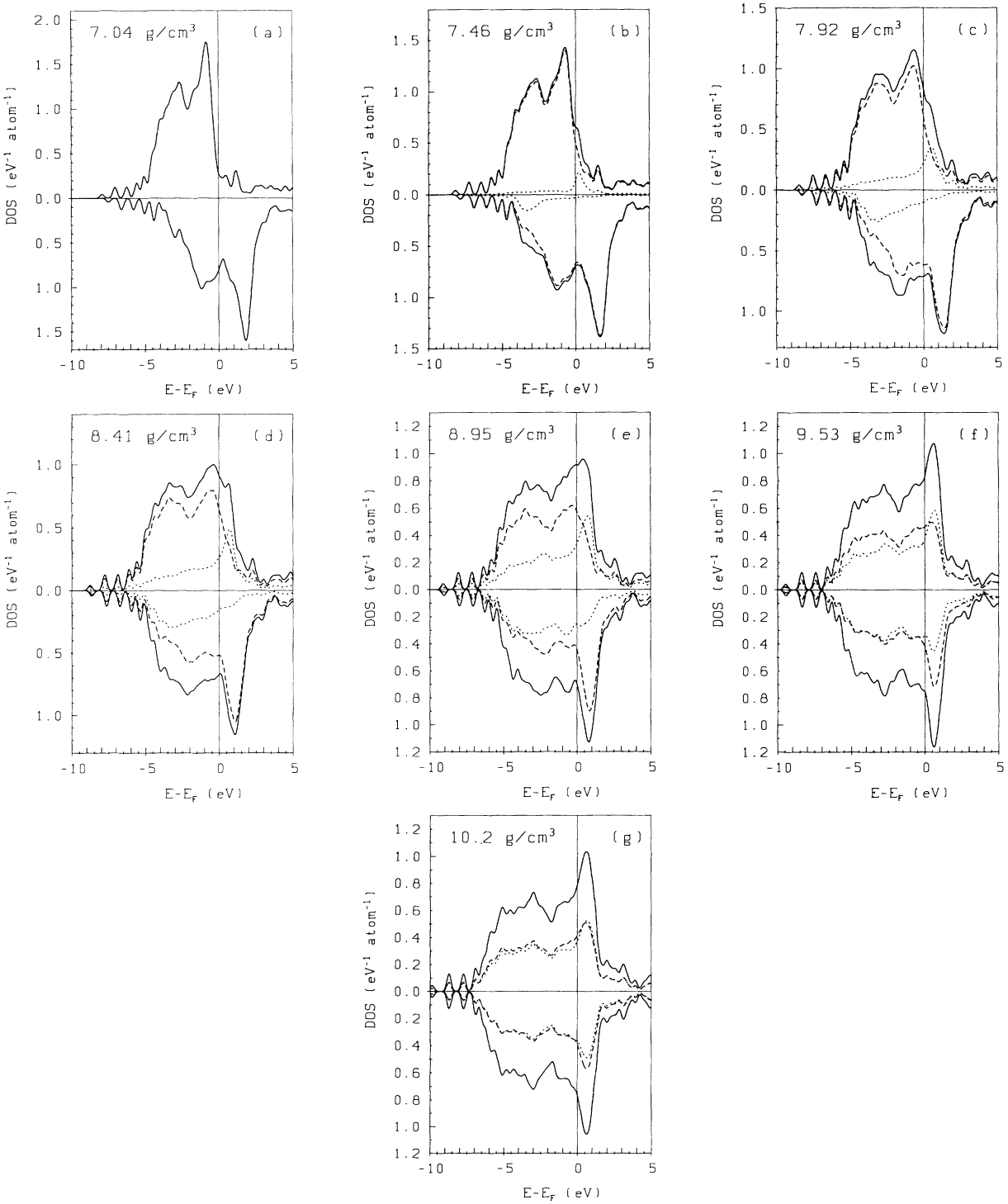

FIG. 10. (a)–(g): Spin-polarized density of states (DOS) for amorphous iron at densities between $\rho = 7.04$ g/cm^3 and $\rho = 10.2$ g/cm^3. Solid line—total DOS, dashed line—average local DOS on the sites with positive magnetic moment, and dotted line—average local DOS on the sites with negative magnetic moment.

ments for amorphous iron at different densities. At the lowest density (where there are no sites with negative moments), amorphous Fe is clearly a strong ferromagnet: the band of the majority spins is completely full; the band of the minority spins is broadened and only about half filled. The DOS on the sites with positive magnetic moments changes only gradually with the Fermi level moving into the majority-spin band, marking the transition from strong to weak ferromagnetism. The DOS at the sites with negative moments is entirely different: the band of the majority (down) spins has the character of a band of resonant bound states of impurities close to the bottom of the host band. Due to the very small width of this band, the exchange splitting is very large, and the main peak of a minority (spin-up) DOS is shifted above the Fermi energy [Fig. 10(b)]. Thus we note that the first appearance of sites with negative moments coincides with the transition from strong to weak magnetism and that the sites with negative moments are characterized by a strong potential acting on the spin-down electrons.

Further compression brings a gradual modification of the electronic DOS: the DOS on the negative moment sites broadens and loses its localized character [Figs. 10(c)–10(e)], and at the density corresponding to the spin-glass regime there is an almost perfect symmetry between the spin-up and spin-down states on the positive and negative moment sites. This picture is distinctly different from the spin-polarized DOS of amorphous Co (Fig. 11). Over a wide range of densities, amorphous Co is found to be a strong ferromagnet, with a completely filled spin-up band. Upon compression, the width of the d band increases and the DOS at the Fermi level is reduced. At very large compression ($\rho = 1.46\rho_{\rm hcp}$), the Stoner criterion of $n(E_F) \geq 1$ state/eV atom spin (see Sec. VII) is no longer satisfied, and a transition to a nonmagnetic state occurs.

VII. EXCHANGE SPLITTING

The most important band property related to magnetism is the magnetic exchange splitting of the states near the Fermi energy, i.e., the $3d$ states in our case. However, when the spin polarization introduces not only a rigid shift of majority and minority bands, but also a substantial distortion of the bands, a quantification of the exchange splitting might be difficult. In this context we find the parametrization of the potential used in the LMTO very useful. In Fig. 12 we plot the $3d$-potential parameters $C_{i\uparrow}$ and $C_{i\downarrow}$ describing the center of the pure spin-up and spin-down $3d$ bands at the site i against the local magnetic moment μ_i. We find that for both majority and minority spins there is a linear relationship between $C_{i\uparrow}$, $C_{i\downarrow}$, and the magnetic moment. The lines representing $C_{i\uparrow}$ and $C_{i\downarrow}$ cross at $\mu_i = 0$, suggesting that the local magnetic splitting is proportional to the local magnetic moment. A least-squares fit to the distributions shown in Fig. 12 gives a proportionality of 0.95 eV/μ_B between the magnetic exchange splitting $(C_{i\downarrow} - C_{i\uparrow})$ and

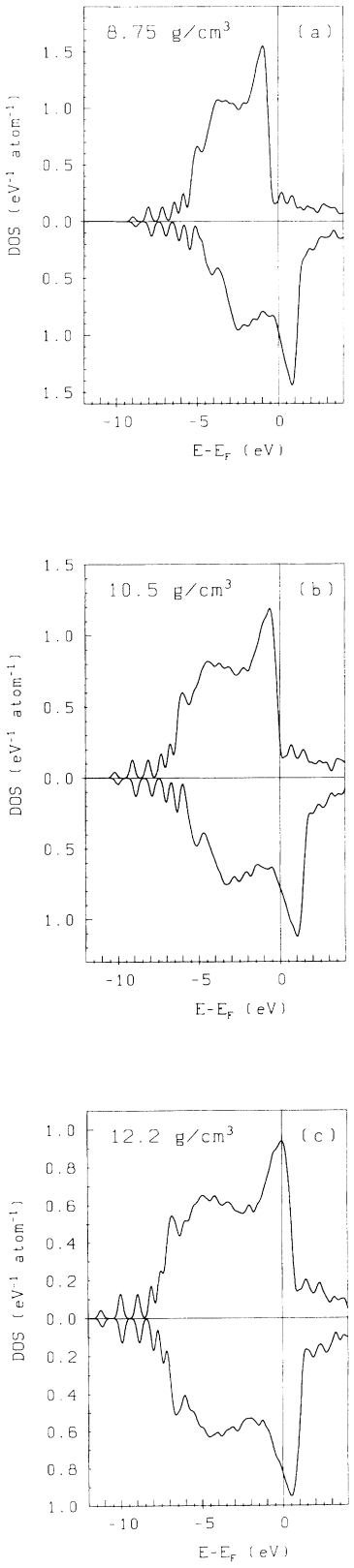

FIG. 11. (a)–(c): Spin-polarized density of states (DOS) for amorphous cobalt at densities between $\rho = 8.75$ g/cm^3 and $\rho = 12.2$ g/cm^3. Solid line—total DOS, dashed line—total spin-up DOS, and dotted line—total spin-down DOS.

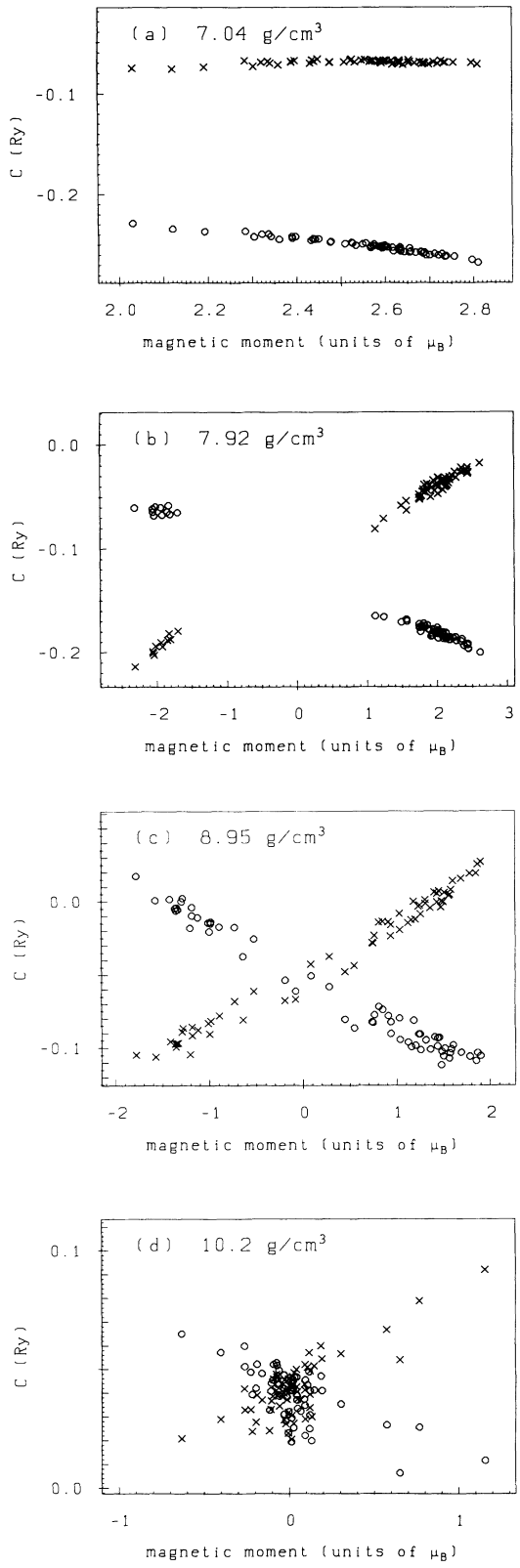

FIG. 12. (a)–(d): Local potential parameters $C_{i\uparrow}$ (circles) and $C_{i\downarrow}$ (crosses) plotted against the local magnetic moment in amorphous iron at different densities between $\rho = 7.04$ g/cm^3 and $\rho = 10.2$ g/cm^3. Note the change of scale for the magnetic moments.

the magnetic moment at all densities. This proportionality is the same for sites with positive and negative moments, and it holds in the ferromagnetic, antiferromagnetic, and spin-glass regimes. Preliminary results suggest that the magnetic exchange splitting per unit of the local magnetic moment is also nearly the same in amorphous Co, and in amorphous Fe-Zr and Co-Zr alloys.[43] Very recently, Himpsel[3] has drawn a similar conclusion from the analysis of photoemission and inverse photoemission data on fcc and bcc Fe overlayers on Ag(100) and Cu(100) substrates (both ferromagnetic), on antiferromagnets (Cr), on spin glasses (AgMn) and free Ni,Co,Fe atoms. The value of 1 eV/μ_B found for the ratio of exchange splitting to magnetic moment is very close to the value of 0.95 eV/μ_B derived from our first-principles calculations.

Within the framework of the theory of itinerant ferromagnets, the ratio of the exchange splitting to the moment is known as the Stoner parameter. The Stoner parameter is essential in determining the magnetic properties such as Curie temperature, magnetization and susceptibility, at least within the Stoner model. Independent of this model, earlier LSD calculations for ferromagnetic $3d$ metals[8–12,26] had shown that the Stoner parameter is approximately 1 eV/μ_B, nearly independent of the metal. The results presented by Himpsel extend this correlation to antiferromagnetic and spin-glass materials; our results show that this correlation holds on a local level even in magnetically disordered materials.

VIII. DISCUSSION

We have presented a fully self-consistent calculation of the electronic and magnetic structure of amorphous iron and cobalt. While our results for the variation of the average magnetic moment with density agree with earlier investigations based on parametrized tight-binding Hamiltonians, significant differences are found in the calculated distribution of the magnetic moments. Expanded amorphous iron (with a density that is about 10% lower than that of bcc iron under normal conditions) is found to be a strong ferromagnet with a rather narrow distribution of the magnetic moments. A slight increase of the density leads to a broadening of the bands and a transition to weak ferromagnetism. The transition from weak to strong ferromagnetism is coupled with the appearance of a few large negative moments. Upon further compression, more moments change sign, and at densities that are 5–10% larger than in bcc iron, the magnetic polarization of amorphous iron has a substantial antiferromagnetic component. The magnetovolume effect leads to a reduction of positive and negative moments, their distributions overlap and finally a transition to a spin-glass phase occurs. This scenario of a transition from a ferromagnetic via an antiferromagnetic to a spin-glass state under compression contrasts with the picture of an inhomogeneous ferromagnetic state at all densities and a general decrease of all magnetic moments as the atomic volume decreases.

The appearance of negative magnetic moments is not

simply correlated to the local atomic volume, the coordination number, the Madelung electrostatic site energy, or any other local quantity. This would suggest that the change in the magnetic properties arises from competing ferromagnetic and antiferromagnetic exchange interactions.

ACKNOWLEDGMENTS

This work was supported by the Bundesministerium für Wissenschaft und Forschung under Contract No. 49.658/3-II/A/4/90 within the framework of the Materials Research Program.

*Permanent address: Institute of Physical Metallurgy, Czechoslovak Academy of Sciences, Žižkova 22, CS-61662 Brno, Czechoslovakia.

[1] G. A. Prinz, Phys. Rev. Lett. **54**, 1051 (1985).
[2] D. P. Pappas, K. P. Kämper, and H. Hopster, Phys. Rev. Lett. **64**, 3179 (1990).
[3] F. J. Himpsel, Phys. Rev. Lett. **67**, 2363 (1991).
[4] C. Lin, E. R. Moog, and S. D. Bader, Phys. Rev. Lett. **60**, 2422 (1988).
[5] M. Maurer, J. C. Dusset, M. F. Ravet, and M. Piecuch, Europhys. Lett. **9**, 803 (1989).
[6] W. Kohn and L. J. Sham, Phys. Rev. **140**, A1133 (1965).
[7] U. von Barth and L. Hedin, J. Phys. C **5**, 1629 (1972).
[8] J. Kübler, Phys. Lett. **81A**, 81 (1981).
[9] C. S. Wang, B. M. Klein, and K. Krakauer, Phys. Rev. Lett. **54**, 1852 (1985).
[10] V. L. Moruzzi, P. M. Marcus, and J. Kübler, Phys. Rev. B **39**, 6957 (1989).
[11] A. R. Jani, G. S. Tripathi, N. E. Brener, and J. Callaway, Phys. Rev. B **40**, 1593 (1989).
[12] J. Kübler, Solid State Commun. **72**, 631 (1989).
[13] O. N. Mryasov, A. I. Liechtenstein, L. M. Sandratskii, and V. A. Gubanov, J. Phys. Condens. Matter **3**, 7683 (1991).
[14] T. Mizoguchi, in *Magnetism and Magnetic Materials (Pittsburgh, 1976)*, Proceedings of the Conference on Magnetism and Magnetic Materials, AIP Conf. Proc. No. 34, edited by J. J. Becker and G. H. Lander (AIP, New York, 1976), p. 286.
[15] J. M. D. Coey, F. Givord, A. Lienard, and J. P. Rebouillat, J. Phys. F **11**, 2707 (1981).
[16] H. Ma, H. P. Kunkel, and G. Williams, J. Phys. Condens. Matter **3**, 5563 (1991).
[17] Y. Kakehashi, Phys. Rev. B **43**, 10 820 (1991).
[18] D. H. Ryan, J. M. D. Coey, E. Batalla, Z. Altounian, and J. O. Strom-Olsen, Phys. Rev. B **35**, 8630 (1987).
[19] N. Saito, H. Hiroyoshi, K. Fukamichi, and Y. Nakagawa, J. Phys. F **16**, 911 (1986).
[20] P. Mathur, Z. Phys. B **53**, 255 (1983).
[21] T. Fujiwara, J. Non-Cryst. Solids **61+62**, 1039 (1984).
[22] U. Krauss and U. Krey, J. Magn. Magn. Mater. **98**, L1 (1991).
[23] Y. N. Xu, Y. He, and W. Y. Ching, J. Appl. Phys. **69**, 5460 (1991).
[24] Ch. Hausleitner and J. Hafner, Phys. Rev. B **42**, 5863 (1990).
[25] Ch. Hausleitner and J. Hafner, Phys. Rev. B **45**, 115 (1992); **45**, 128 (1992).
[26] O. K. Andersen, O. Jepsen, and D. Glötzel, in *Highlights of Condensed Matter Theory*, edited by F. Bassani, F. Fumi, and M. P. Tosi (North-Holland, Amsterdam, 1985), p. 59.
[27] H. L. Skriver, *The LMTO Method* (Springer, Berlin, 1984).
[28] S. S. Jaswal and J. Hafner, Phys. Rev. B **38**, 7311 (1988).
[29] W. Jank, Ch. Hausleitner, and J. Hafner, Europhys. Lett. **16**, 473 (1991).
[30] Ch. Hausleitner, G. Kahl, and J. Hafner, J. Phys. Condens. Matter **3**, 1589 (1991).
[31] T. Ichikawa, Phys. Status Solidi A **19**, 707 (1973).
[32] O. K. Andersen, O. Jepsen, and M. Šob, in *Electronic Band Structure and Its Applications*, Lecture Notes in Physics, Vol. 283, edited by M. Yussouff (Springer, Berlin, 1987), p. 1.
[33] S. K. Bose, S. S. Jaswal, O. K. Andersen, and J. Hafner, Phys. Rev. B **37**, 9955 (1988).
[34] T. Jarlborg and M. Peter, J. Magn. Magn. Mater. **42**, 89 (1984).
[35] P. Blaha, K. Schwarz, and P. H. Dederichs, Phys. Rev. B **38**, 9368 (1988).
[36] V. L. Moruzzi, J. F. Janak, and A. R. Williams, *Calculated Electronic Properties of Metals* (Pergamon, New York, 1978).
[37] J. F. Janak, Solid State Commun. **25**, 53 (1978).
[38] J. L. Finney, Proc. R. Soc. London, Ser. A **319**, 479 (1970).
[39] W. Brostow, Chem. Phys. Lett. **49**, 285 (1977); W. Brostow, J. P. Dussault, and B. L. Fox, J. Comp. Phys. **28**, 81 (1978).
[40] T. Egami, K. Maeda, and V. Vitek, Philos. Mag. A **41**, 883 (1981).
[41] J. Hafner, in *Structure of Non-crystalline Materials II*, edited by P. H. Gaskell and E. A. Davies (Taylor and Francis, London, 1983), p. 539.
[42] K. Huang, Proc. R. Soc. London, Ser. A **203**, 178 (1950).
[43] I. Turek, Ch. Becker, and J. Hafner (unpublished).